# MEDUSE: 10 GHz localized quasi-planar wave measuring bench in order to analyse systems electromagnetic susceptibility

Sami Barouki, Patrick Hoffmann, Alain Reineix

# MEDUSE: 10 GHz localized quasi-planar wave measuring bench in order to analyse systems electromagnetic susceptibility

*Note: Sub-titles are not captured in Xplore and should not be used


Sami Barouki
French Alternatives Energies and Atomic Energy Commission
CEA DAM Gramat,
Gramat, France
sami.barouki@cea.fr

Patrick Hoffmann
French Alternatives Energies and Atomic Energy Commission
CEA DAM Gramat,
Gramat, France
patrick.hoffmann@cea.fr

Alain Reineix
Xlim Research Institute
CNRS UMR 7252
Limoges, France
alain.reineix@xlim.fr



***Abstract*—This paper outlines the design of a focused plane-wave illumination bench for studying the electromagnetic susceptibility of electronic systems. The bench consists of a horn antenna and a dielectric lens used to focus plane wave in the X-band at 10 GHz.**



***Keywords—RF DEW, dielectric, lens, antenna, EMS, RFI, plane wave, coupling, infrared thermography, electromagnetic field***


## I. Introduction

In our hyper connected world, the proliferation of electronic devices has led to a growing dependence on them, prompting analysis of an emerging threat; radio frequency directed energy weapons (RF DEW). RF DEWs are intentional sources of electromagnetic (EM) aggression that generate radio frequency interferences (RFI) and disrupt the normal operation of electronic equipment. By considering specific frequencies and time domain, RF DEWs are able to generate temporary or permanent damage on targets, the key element of which is the electronic component.

Electromagnetic susceptibility (EMS) studies are part of research activities carried out on RF DEW at the CEA Gramat. They consist of researching, understanding and anticipating the physical phenomena generated on electronic systems by RF DEWs.

Electronic systems becoming increasingly complex, an electromagnetic attack generates a global effect on these systems. Then it is difficult to extract the different physical phenomena that are produced and therefore to develop unitary models able to reproduce the behavior. In this context, the CEA Gramat has been working for many years to develop different approaches for analyzing the susceptibility of systems:

- Plane wave illumination makes it possible to assess the overall vulnerability of a system and to approximate a real scenario. This approach is very efficient but presents many difficulties in differentiating the effects on the parts of the system and increases the difficulty of modelling.
- Near-field illumination makes it possible to localise the attack on a precise part of the system without being intrusive. The main drawback is the difficulty to assess the characteristics of the temporal waveform of the attack. This makes it difficult to estimate the threat signal in far field; moreover, the power delivered is limited.
- Direct power injection (DPI) allows the generation of the attack on a precise point of the system (or a component). We have an exact knowledge of the temporal shape of the injected signal, with important precision, but it is often invasive and generally requires a physical intervention on the electronic equipment.

The objective of this study is to introduce a complementary approach to the previous ones. The aim is to produce a system illumination laboratory prototype (MEDUSE: Moyen d'Emission Dédié Ultrafocalisé pour la Susceptibilité Electromagnétique) able to generate a electromagnetic plane wave radiation. The characteristics of this wave are: a knowledge of the analytical expression of the temporal waveform, a small illumination area (close to one $cm^2$) and non-test.

The measuring bench consists of a conical horn antenna and a focusing lens. In order to validate our measuring bench, we carried out intrusive a series of measurements summarized as follows on Fig. 1.

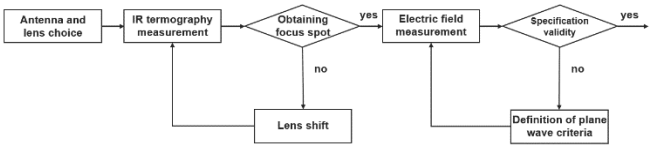


Fig. 1. Flow chart of the experimental process

This article introduces the methods used to verify the two essential points, i.e. the characterization of the attack in the form of a plane wave and the focusing parameters of the device.

## II. Mesurement techniques and results

### A. Infrared thermography measurements

This type of measurement will enable us to characterize the focus of the MEDUSE device. Measurement by infrared thermography consists of measuring the heating of a film due to the coupling between an electric field and a thin conductive film following electromagnetic illumination. This heating is measured using an infrared camera and is based on the following considerations.

Any amount of heat applied to a material satisfies the heat equation:

$$-\kappa\Delta\mathrm{T} + \rho c_p \frac{\partial T}{\partial t} = -p_s(t)$$

Where κ is the thermal conductivity of the film, ρ is its bulk density and $c_p$ is its specific heat at constant pressure. As for $p_s$, this is the source term expressed in term of applied volume power density

The solutions of equation described in [3] and [4] will be applied on a disc of radius r located on the illuminated film:

$$\varepsilon = 4\pi r^2 \sqrt{\rho c_p \kappa t} \cdot (T - T_0) \quad (1)$$

ε is the incident energy presented to the film on the disc to reach the temperature *T*; t is the exposure time and $T_0$, the initial temperature of the film before the energy stress be applied.

The energy applied is derived in our case from an electromagnetic plane wave characterized by an electric field $\vec{E}$. The induced volume power density applied to the film is: $\vec{J} \cdot \vec{E}$; $\vec{J}$ *S* the surface density of the current flowing through the film. Thus, the electrical energy due to the electromagnetic signal is:

$$\varepsilon = \vec{J} \cdot \vec{E} \cdot S \cdot w_F \cdot t \quad (2)$$

*S* is the surface on which the electromagnetic field is applied, i.e. the surface of the film, and $w_F$ is its thickness (or its skin depth $\delta_s$ if $\delta_s < w_F$). If we assume that all this energy results in heating of the film, then:

$$\varepsilon = \sigma\vec{E} \cdot \vec{E} \cdot S \cdot w_F \cdot t = \sigma\left\|\vec{E}\right\|^2 \cdot S \cdot w_F \cdot t \quad (3)$$

So, introducing (3) into (1), we obtain:

$$\left\|\vec{E}\right\| = \sqrt{\frac{4\pi r^2}{S}} \cdot \sqrt{\frac{1}{\sigma w_F}} \cdot \sqrt[4]{\frac{\rho c_p \kappa}{t}} \cdot \sqrt{T - T_0} \quad (4)$$

Let:

$$\left\|\vec{E}\right\| = k \cdot \sqrt{\Delta T} \quad (5)$$

In equation (4), the zone impacted by the heating effect and represented by the disc of radius r is subject to diffusion phenomena. An illumination time must be chosen to obtain good temperature sensitivity necessary to determine the value of the field and to minimise the diffusion phenomenon in order to determine the focusing spot. The illumination time was set at 5 seconds for all the experiments. In these experiments, it was not so much the electric field values that were important to us, but those of the radius of the focal spot $r_f$, the focal distance df between lens and film and also the far-field distance $d_{CL}$ between antenna and lens (6).

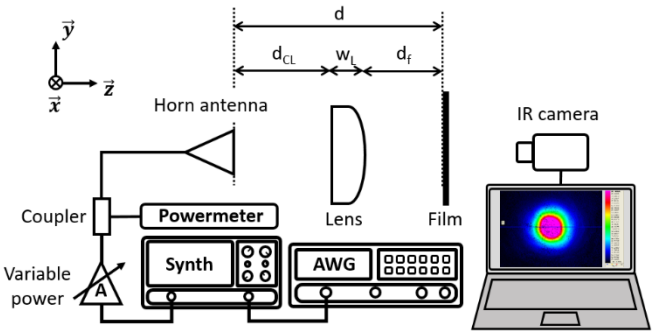


Fig. 2. Infrared thermography measurement bench

The measurement set-up is shown in Fig.2. The emitting part consists of a specially designed horn antenna operating at a frequency of 10 GHz (λ is its wavelength in vacuum). A plano-convex PLA dielectric lens of diameter D is placed at a distance $d_{CL}$ such that the field incident on its flat surface has far-field characteristics. A synthesizer and an arbitrary generator (AWG) are used to shape the emission signal. A 400 W (continuous wave: CW) amplifier is used to amplify the incident signal and a powermeter reads the power on the amplifier's coupled channel. The receiving section is constituted by a film made of carbon-filled polymers (Kapton) and an infrared camera. The minimum distance adopted for the far field is defined by:

$$\mathrm{d_{CL}} \geq {2\mathrm{D}^2}/{\lambda} \quad (6)$$

The advantages of this measurement method are on the one hand the speed of implementation and on the other hand visualization of the field mapping. The main drawback is access to a relative value of the electric field (a reference measurement must be carried out with another means to determine the real value of the field). The results of these measurements are above all qualitative, but above all extremely visual, enabling the positions of each entity in the experimental chain to be determined very quickly.

### *B. Results of infrared thermography measurements*

The aim of the measurements is to determine the diameter of the illumination spot at focal length $d_f$. The method used to determine the size of this illumination spot is as follows:

Electromagnetic illumination duration is 5 seconds preceded by a 500 ms “cold time” to define the initial temperature $T_0$ and the associated color by the infrared camera processing software. A color scale is determined at the end of the measurement. Each color change indicates, for a certain time (number of images), the space region where electromagnetic energy is present, before undergoing the diffusion phenomenon that enlarges the impacted thermal zone before the color fades. It is this measurement of the number of pixels in this zone, reduced to a geometric quantity that enables us to measure the illumination spot. The following images illustrate this method.

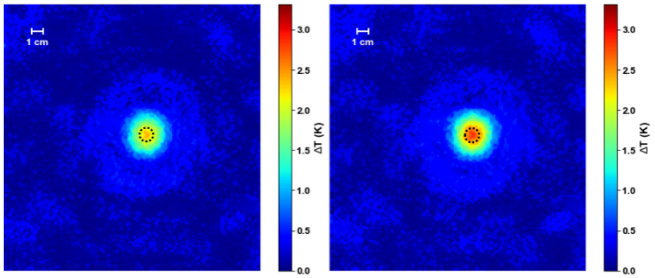


Fig. 3. Measurement of the illumination spot (temperature homogeneous zone circled in black dotted line). a) measurement at t=3.9s, ΔT≈2.5K. b) measurement at t=5s, ΔT≈3K

Measurements carried out on a large number of images and experiments enabled us to measure an illumination area such as its radius $r_f = 5.5$ mm.

Numerical simulation of the device using the CST Studio Suite tool enabled us to compare similar results between simulation and experimentation.

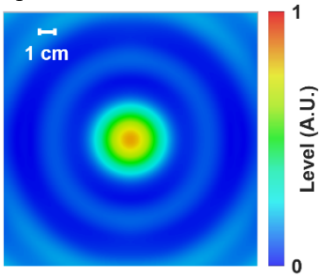


Fig. 4. Simulation result on CST at distance $d_f$

## C. *Electric field measurements*

As previously mentioned, the electric field is measured by a second processing chain (Fig.5). The electromagnetic field is emitted and received by identical antennas developed specifically using a 3D printing process (Fig.6).

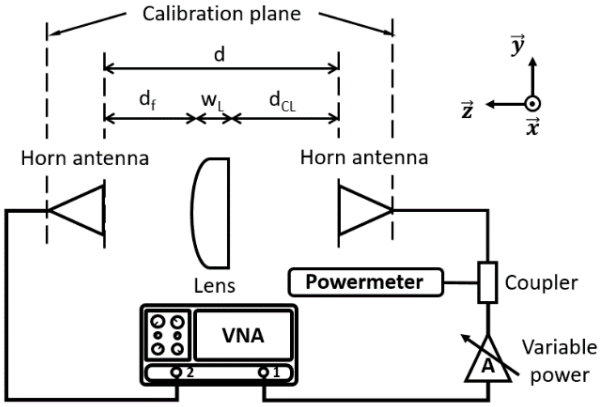


Fig. 5. Electric field measurement bench

These antennas were measured on antenna characterization platform of the CEA Gramat (Fig.6).

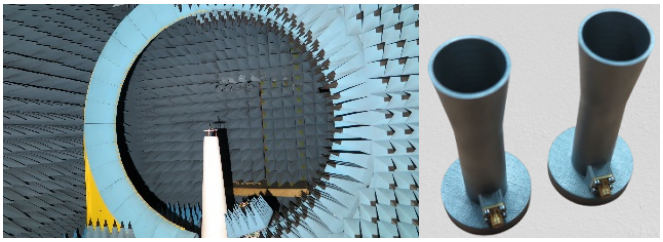

Fig. 6. CEA Gramat's antenna measurement base and antennas integrated into the measurement chain

Fig. 8 shows a 3D view of the radiation pattern of the antennas measured in the antenna base, used for the reference measurement.

An initial measurement is carried out between the two antennas under plane-wave conditions without a lens, to check the gain value in the positive z direction and ensure the mechanical accuracy of the experimental bench supporting the antennas, lens and thermal film (Fig. 7).

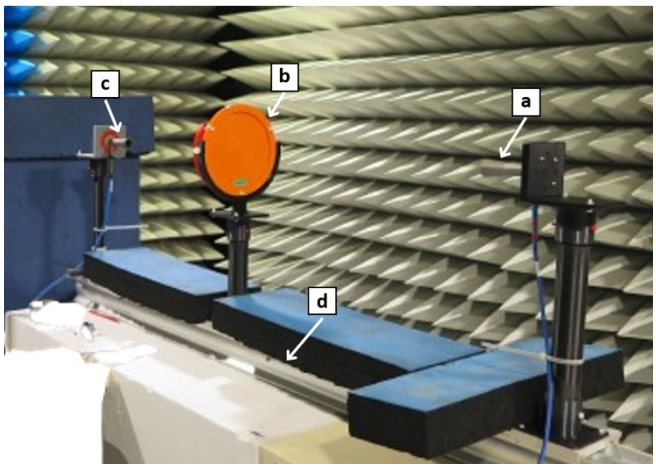


Fig. 7. Photo of test bench. a) emitting antenna; b) PLA lens; c) receiving antenna; d) alignment guide

The two antennas are positioned identically to ensure optimum polarization efficiency. The power balance between these two antennas is expressed by the usual Friis formula:

$$G_e \cdot G_r = G^2 = \left(\frac{4\pi}{\lambda}\right)^2 \cdot \frac{P_r}{P_e} \cdot d^2 \qquad (7)$$

$G_e$ ($P_e$) and $G_r$ ($P_r$) being respectively the transmitting antenna gain (the power at the base of the transmitting antenna) and the receiving gain (the power at the base of the receiving antenna). The gains are identical *(G)*; d is the distance between the two antennas. After taking into account the losses of the various cables, the measured gain is exactly the one characterized in the antenna measurement base (Fig.5), enabling us to check the precision of the alignment of the various elements of the experimental bench.

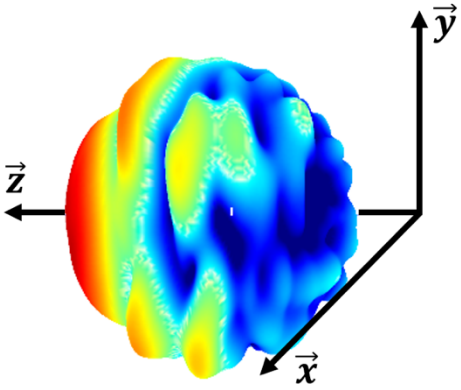


Fig. 8. Experimental 3D radiation pattern in $E_{total}$ of reference antennas

A set of measurements is then made with the lens to determine the device's gain relative to the reference measurement, and the decay of this gain as it moves along the

x-axis, in order to assess the size of the illumination surface. The bench is shown in Fig.5.

It consists of a vector network analyzer (VNA), a conical horn antenna on transmitting part (the one used as the source in the first bench), an identical received antenna and a 400W (CW) amplifier.

The results of the device's gain measurement are shown in Fig.9.

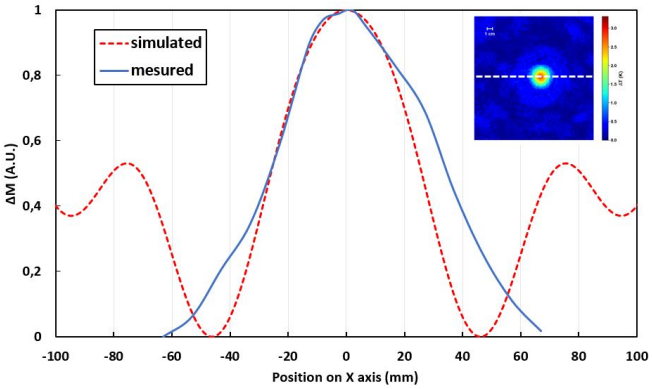


Fig. 9. Measurement of device level as function of lateral distance from a centered alignment

The linear value of the device gain is estimated around 14 dB. This value remains an estimate, as the effective area of the receiving antenna is greater than the focal spot resulting from the infrared measurement ($A_e$ = 2.5 cm² for the antenna, $A_s \leq$ 1 cm² for the focal spot). We can note the rapid decreases in gain outside the focal spot, further confirming the size of this area.

In addition, a free-space electric field probe (Prodyn AD-20R) was used at reception to measure the contribution of the z-following component of the electric field. This shows an attenuation of 25 dB compared with the transverse field components (in x and y), demonstrating the planar nature of the electric field reaching the focal distance.

## III. Conclusion

On the basis of our results, we have demonstrated that the electromagnetic wave can be focused onto a surface area of around 1 cm² at the focal length of the lens, while maintaining the plane-wave characteristics for the illumination. Future experiments will enable us to apply this concept to the analysis of the electromagnetic susceptibility of an electronic board: localized electromagnetic aggression and control of the expression of the incident waveform, a prerequisite for the search for a physical model of electromagnetic susceptibility.

## Acknowledgment

Research financially supported by the French Ministry of Defence – Defence Innovation Agency.

## References

[1] Y. T. Lo, S. W. Lee, Antenna Handbook, Theory Applications, and Design, Volume 1, Springer Science+Business Media New York, 1988.J. Clerk Maxwell, A Treatise on Electricity and Magnetism, 3rd ed., vol. 2. Oxford: Clarendon, 1892, pp.68–73.

[2] D. Prost, F. Issac, F. Lemaître, J. P. Parmentier, “Infrared Thermography of Microwave Electromagnetic Fields”, International Symposium on Electromagnetic Compatibility – EMC Europe, Rome, Italy, 2012, pp.1-4.

[3] H. S. Carslaw, J. C. Jaeger, “Conduction of Heat in Solids”, Oxford University Press, 1959

[4] D. Wunsch, R. Bell, “Determination of threshold failure levels of semiconductor diodes and transistors due to pulse power voltages, IEEE Transactions on Nuclear Science, Vol. 15, pp 244-259, 1968